Second-Order Sliding Mode Strategy for Air–Fuel Ratio Control of Lean-Burn SI Engines

Behrouz Ebrahimi, *Member, IEEE*, Reza Tafreshi, *Member, IEEE*, Javad Mohammadpour, *Member, IEEE*, Matthew Franchek, *Member, IEEE*, Karolos Grigoriadis, *Senior Member, IEEE*, and Houshang Masudi

***Abstract*— Higher fuel economy and lower exhaust emissions for spark-ignition engines depend significantly on precise air–fuel ratio (AFR) control. However, the presence of large time-varying delay due to the additional modules integrated with the catalyst in the lean-burn engines is the primary limiting factor in the control of AFR. In this paper, the engine dynamics are rendered into a nonminimum phase system using Padé approximation. A novel systematic approach is presented to design a parameter-varying dynamic sliding manifold to compensate for the instability of the internal dynamics while achieving desired output tracking performance. A second-order sliding mode strategy is developed to control the AFR to remove the effects of time-varying delay, canister purge disturbance, and measurement noise. The chattering-free response of the proposed controller is compared with conventional dynamic sliding mode control. The results of applying the proposed method to the experimental data demonstrate improved closed-loop system responses for various operating conditions.**

***Index Terms*— Air–fuel ratio (AFR) control, dynamic sliding manifold, lean-burn engine, nonminimum phase system, second-order sliding mode, time-varying delay.**

I. Introduction

LEAN-BURN spark-ignition engines exhibit significant performance enhancement in terms of tailpipe emissions and fuel economy compared with the common spark-ignition engines. They operate at up-stoichiometric air–fuel ratio (AFR) leading to reduced carbon monoxide and hydrocarbons but increased nitrogen oxide (NO_x) levels. The excessive NO_x is stored in the lean NO_x trap (LNT) module, which is integrated with the three-way catalyst (TWC) downstream the universal exhaust gas oxygen (UEGO), as shown in Fig. 1. The stored NO_x is released after reaching a certain threshold while simultaneous switching of the engine into rich operation converts it to nonpolluting nitrogen. Although this process leads to a significant reduction in harmful emissions, it introduces a larger time-varying delay for the gas exiting the cylinder to reach the UEGO sensor. The large time delay, however, restricts the closed-loop system's stability and bandwidth. Moreover, wide range of engine operating conditions, the inherent nonlinearities of the combustion process, the large modeling uncertainties, and parameter variations pose further challenges to the design of the control system for lean-burn engines.

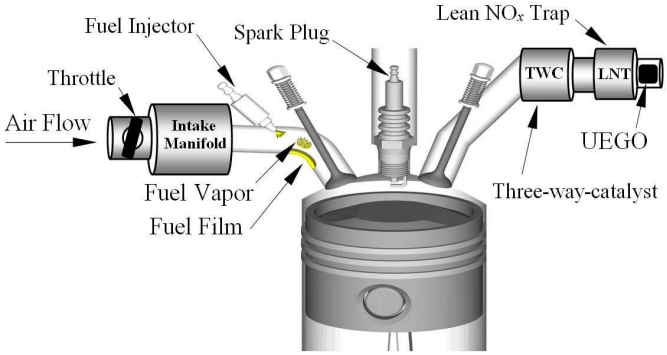

Fig. 1. System configuration of a lean-burn engine.

There has been a great amount of research to address the AFR control problem. However, a more sophisticated control approach is needed to accurately maintain the engine AFR close to the target value in the presence of time-varying delay, uncertainties, and measurement noise. Linear control schemes have been presented based on design techniques such as linear quadratic Gaussian [1], H_∞ control [2], linear parameter-varying (LPV) control [3], proportional–integral–derivative (PID) control [4], [5], model predictive control [6], and gain-scheduling (GS) method [7]. The following nonlinear strategies have been also considered: sliding mode control (SMC) [8], [9], [10], [11] and its higher order schemes (HOSMC) [12], fuzzy-based techniques [13], adaptive posicast control (APC) [14], and neural networks (NNs) [15].

Among the nonlinear robust controllers, SMC is one of the most widely studied control schemes for engine control applications due to its intrinsic characteristics against inherent

Manuscript received July 23, 2012; revised June 26, 2013; accepted August 20, 2013. Manuscript received in final form September 8, 2013. Date of publication September 26, 2013; date of current version June 16, 2014. This work was supported by the Qatar National Research Fund NPRP under Grant 08-398-2-160. Recommended by Associate Editor J. Y. Lew.

B. Ebrahimi, R. Tafreshi, and H. Masudi are with the Mechanical Engineering Program, Texas A&M University, Doha 23874, Qatar (e-mail: behrouz.ebrahimi@qatar.tamu.edu; reza.tafreshi@qatar.tamu.edu; houshang.masudi@qatar.tamu.edu).

J. Mohammadpour is with the College of Engineering, University of Georgia, Athens, GA 30602 USA (e-mail: javadm@gmail.com).

M. Franchek and K. Grigoriadis are with the Department of Mechanical Engineering, University of Houston, Houston, TX 77204 USA (e-mail: mfranchek@central.uh.edu; karolos@uh.edu).

Color versions of one or more of the figures in this paper are available online at http://ieeexplore.ieee.org.

Digital Object Identifier 10.1109/TCST.2013.2281437

nonlinearities of the combustion process, the large modeling uncertainties, and parameter variations. A conventional sliding mode controller was presented by Cho and Hedrick [8], which could only guarantee the attractiveness of the switching surface within a boundary layer in the vicinity of the surface. The boundary layer thickness was built upon the delay that could yield significant tracking error for large delays as in lean-burn engines. Later, a follow-up paper proposed an observer-based sliding mode controller to improve the chattering effect [9]. Furthermore, adaptive SMC using Gaussian NN has been used to update the fueling parameters and air flow into the cylinders to compensate for the transient fueling dynamics [10].

Although SMC is robust against uncertainties and nonlinearities, it suffers from the chattering dilemma, which is a high-frequency oscillation over the switching surface. To circumvent this problem, a second-order sliding mode controller (SOSMC), which preserves the robustness characteristics of the conventional SMC while reduces the chattering effect has been reported for the AFR control problem [12]. In the proposed control approach, a radial basis function has been used to adjust the slope of the sliding surface. The research on SOSMC is ongoing to fully use its potential for the engine parameter estimation and control purposes [16].

Aforementioned control schemes have been developed on spark-ignition engines considering cycle delay due to the four strokes of the engine. However, for lean-burn engines, the gas transport delay caused by the exhaust gas flowing from the exhaust valve into the tailpipe UEGO sensor results in additional delays. An LPV GS controller has been designed in [3] for the AFR control of a lean-burn engine, where a prefilter has been employed to extend the closed-loop AFR tracking bandwidth. Furthermore, the scheduling parameters have been explicitly represented for a specific engine model [3]. A more systematic approach to control AFR in lean-burn engines has been reported using a PID controller, where a dynamic filter has been proposed to compensate for the delay effects [4].

In this paper, a SOSMC will be developed for AFR control of lean-burn engines using a parameter-varying dynamic sliding manifold. The lean-burn engine dynamics with large time-varying delay will be first modeled by the Padé approximation. This will represent the system in the form of a nonminimum phase system with parameters changing according to the time-varying delay. The system will be then explored to obtain internal dynamics and input/output pairs. A parameter-varying sliding manifold will be derived explicitly based on the delay. A super-twisting SOSMC will be invoked to drive the surface and its derivative to zero while removing the chattering effect. Variability of the operating conditions including fuel purge disturbance, delay estimation errors, and UEGO sensor noise will be discussed and the performance of the proposed controller will be evaluated.

Section II will briefly present the system modeling for the AFR dynamics. SOSMC along with the associated parameter-varying sliding manifold will be derived in Section III. Results will be discussed in Section IV. Section V will conclude this paper.

II. System Model for AFR Dynamics

Fig. 1 shows the system configuration consisting of throttle, air path, fuel path, TWC, LNT, and UEGO sensor downstream the engine. AFR is influenced by the air flow passing through the intake manifold and the fuel injected by the fueling system. The fueling system includes fuel vapor and fuel wet film dynamics, whose output depends on the fraction of the injected fuel forming the wet film and evaporated fuel from the wet wall. As a common practice in the experimental settings, a compensator is added to the feedforward path to compensate for the fuel wall wetting effect. Estimation approaches based on the least-squares method to obtain fueling system parameters have been proposed in [17] and [18].

The main challenge in the design of an AFR control system for lean-burn engines is the presence of a large time delay due to the location of the UEGO sensor downstream the LNT module. This introduces considerable time delay for the gas to be transported to the UEGO sensor. The gas transport delay is identified as the time that it takes for the exhaust gas to reach the tailpipe UEGO sensor downstream the LNT and can be approximated by $\tau_g = \vartheta/\dot{m}_a$ for an average exhaust temperature, where $\dot{m}_a$ is the air mass flow and ϑ is a constant that should be determined based on the experimental data [3]. In addition, the engine operating envelope such as the engine speed contributes to cycle delay τ_c. The cycle delay is estimated by one engine cycle due to the four strokes of the engine as $\tau_c = 720/(360/60)N = 120/N$[s], where N is the engine speed in rpm. Hence, the overall time delay is given by $\tau = \tau_c + \tau_g$, which is time varying depending on the engine operating condition. The UEGO sensor dynamics can be modeled as a first-order lag $G(s) = 1/(\tau_s s + 1)$. Then, the system open-loop dynamics including UEGO sensor dynamics and the total delay can be described as [4]

$$\tau_s \dot{y}(t) + y(t) = u(t - \tau) \tag{1}$$

where $y(t)$ and $u(t)$ are the measured and input AFR, respectively.

III. Second-Order SMC

The proposed structure of the closed-loop system in this paper is shown in Fig. 2, which consists of the feedforward air-path and fuel-path dynamics. The air-path model estimates the amount of air mass flowing into the combustion chamber using the throttle air mass flow voltage, V_{MAF}, whereas the fuel-path model estimates the amount of fuel mass flow entering into the cylinder. An extensive work on air and fuel characteristics along with a feedforward approach to explore transient air-path and fuel-path dynamics has been reported in [19].

The control design objective is to track the desired AFR in the presence of matched and unmatched disturbances such as fuel injector and canister purge perturbations, unmodeled dynamics, and UEGO sensor measurement noise. Furthermore, the control system structure should be appropriate to be easily implemented in practical settings. In the following, we will first approximate the engine delay to transform the infinite-dimensional problem into a finite-dimensional one. To

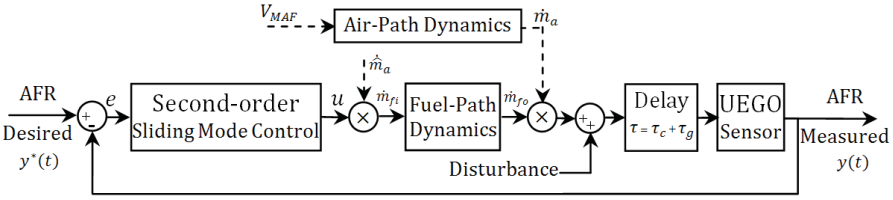

Fig. 2. Closed-loop system structure with the proposed SOSMC.

overcome the shortcoming of the classical SMC in dealing with internally unstable dynamics, a linear dynamic parameter-varying sliding manifold is proposed in this paper to provide the control system with stability and robustness against matched and unmatched perturbations and UEGO measurement noise.

A. Delay and Internal Dynamics

The pure infinite-dimensional time delay system may be approximated by the Padé approximation, which results in a finite-dimensional closed-form representation. In this paper, we have used a first-order Padé approximation because a higher order approximation increases the complexity of the system model and hence the computational cost. Using the first-order Padé approximation, the system (1) can be rewritten as

$$\frac{Y(s)}{U(s)} \cong \frac{1-\frac{\tau}{2}s}{(1+\frac{\tau}{2}s)(1+\tau_s s)} \tag{2}$$

where τ is the overall time-varying delay consisting of cycle delay and exhaust gas transport delay, as explained in Section II. Equation (2) represents a nonminimum phase system due to the presence of a right-half-plane zero caused by the delay. The state-space representation of (2) can be expressed as

$$\begin{aligned} \dot{x}_1(t) &= x_2(t) \\ \dot{x}_2(t) &= -a_0(\tau)x_1(t) - a_1(\tau)x_2(t) + u(t) \\ y(t) &= b_0(\tau)x_1(t) + b_1(\tau)x_2(t) \end{aligned} \tag{3}$$

where $a_0(\tau) = b_0(\tau) = 2(\tau_s\tau)^{-1}$, $a_1(\tau) = (2\tau_s + \tau)(\tau_s\tau)^{-1}$, and $b_1(\tau) = -\tau_s^{-1}$ are the parameter-dependent coefficients. The internal dynamics along with the input/output dynamics of the system may be obtained by the normal form transformation $W = \mathcal{N}(x(t))$, in which, $W = [\xi(t) \quad \eta(t)]^T$ and $\mathcal{N}(x) = [y(t) \quad x_1(t)]^T$ [20]. The corresponding input/output and internal dynamics can be obtained using Lie notation as

$$\begin{aligned} \dot{\eta}(t) &= \mathcal{L}_f\mathcal{N}(x(t)) \\ \dot{\xi}(t) &= \mathcal{L}_f h(x(t)) + \mathcal{L}_g h(x(t))u(t) \end{aligned} \tag{4}$$

where $f(x(t)) = [x_2(t) \quad -a_0(\tau)x_1(t) - a_1(\tau)x_2(t)]^T$, $g(x(t)) = [0 \quad 1]^T$, $h(x(t)) = b_0(\tau)x_1(t) + b_1(\tau)x_2(t)$ and $\mathcal{N}$ is found such that $\mathcal{L}_g\mathcal{N}(x(t)) = 0$. Hence, internal dynamics and input/output pairs are obtained as follows:

$$\dot{\eta}(t) = a_{11}(\tau)\eta(t) + a_{12}(\tau)\xi(t) + \phi_\eta(t) \tag{5a}$$

$$\dot{\xi}(t) = a_{21}(\tau)\eta(t) + a_{22}(\tau)\xi(t) + \beta(\tau)u(t) + \phi_\xi(t) \tag{5b}$$

$$y(t) = \xi(t) \tag{5c}$$

where $a_{11}(\tau) = 2\tau^{-1}$, $a_{12}(\tau) = -\tau_s$, $a_{21}(\tau) = (8\tau_s + 4\tau)(\tau_s\tau)^{-2}$, $a_{22}(\tau) = -(4\tau_s + \tau)(\tau_s\tau)^{-1}$, and $\beta(\tau) = -\tau_s^{-1}$ are corresponding coefficients according to the above transformation. The unstable eigenvalue for the zero dynamics based on $\xi = 0$, which demonstrates instability of the internal dynamics of (5a) for all positive time delays, is equal to $2\tau^{-1}$. We have also included $\phi_\eta(t)$ and $\phi_\xi(t)$ as bounded nonlinear unmatched and matched uncertainties, respectively, to implement a generic control approach that is able to accommodate both unmatched and matched disturbances. The overall system model can also be represented in the following form, which relates the output AFR to the engine input while including the matched and unmatched disturbances

$$\begin{aligned} \beta(\tau)\left[\dot{\bar{u}}(t) - a_{11}(\tau)\bar{u}(t)\right] &= \ddot{y}(t) - \left[a_{11}(\tau) + a_{22}(\tau)\right]\dot{y}(t) \\ &\quad -\left[a_{12}(\tau)a_{21}(\tau) - a_{11}(\tau)a_{22}(\tau)\right]y(t) - a_{21}(\tau)\phi_\eta(t) \end{aligned} \tag{6}$$

where $\bar{u}(t) = u(t) + \beta^{-1}(\tau)\phi_\xi(t)$.

B. Linear Dynamic Parameter-Varying Sliding Manifold

SMC in its conventional form cannot be used for nonminimum phase systems due to the instability in the internal dynamics that leads to the control input to diverge to infinity [21].

To circumvent this problem, a linear dynamic parameter-varying sliding manifold is proposed in this paper to compensate for the unstable internal dynamics of the nonminimum phase system as

$$\chi(t) = \eta(t) + \frac{\sum_{i=0}^{n-1} p_i(\tau)s^i}{s^{n+1} + q(\tau)s^n}e(t) = 0 \tag{7}$$

where $s = d/dt$, $e(t) = y^*(t) - \xi(t)$, and $y^*(t)$ is the desired AFR. The order of the switching manifold n and parameter-dependent coefficients $q(\tau)$ and $p_i(\tau)$ can be determined based on the desired error system dynamics as

$$\left[s^{n+1} + \sum_{i=0}^{n} c_i s^i\right]e(t) = 0. \tag{8}$$

The system motion on the sliding surface (7) for internal dynamics (5a) yields

$$\begin{aligned} &\left\{s^{n+1} + q(\tau)s^n - a_{12}^{-1}(\tau)\sum_{i=0}^{n-1} p_i(\tau)\left[s^{i+1} - a_{11}(\tau)s^i\right]\right\}e(t) \\ &\qquad = \left\{a_{12}^{-1}(\tau)[s^{n+1} + q(\tau)s^n]\right\}\bar{\phi}(t) \end{aligned} \tag{9}$$

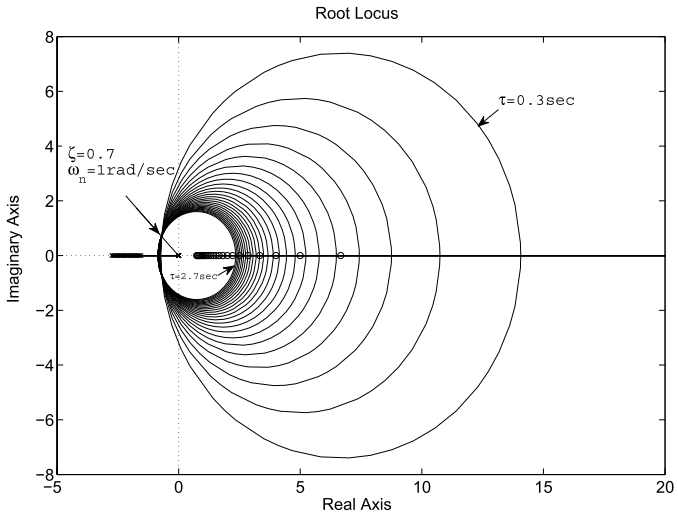

Fig. 3. Engine dynamics on the switching manifold for a sequence of time delays with increments of 0.1s, 0.3s $\leq \tau \leq$ 2.7s.

where $\bar{\phi}(t) = a_{12}(\tau)y^*(t) + \phi_\eta(t)$. It can be assumed that $\bar{\phi}$ is a bounded smooth function, whose nonzero kth-order time derivative is zero, i.e., $(d^k/dt^k)\bar{\phi}(t) \equiv 0$, and $k \leq n$. Hence, the right-hand side in (9) is vanished and the zero steady-state tracking error is achieved

$$\left\{s^{n+1} + q(\tau)s^n - a_{12}^{-1}(\tau)\sum_{i=0}^{n-1} p_i(\tau)\left[s^{i+1} - a_{11}(\tau)s^i\right]\right\}e(t) = 0. \tag{10}$$

By rearranging (10) in descending order of derivatives and equating the corresponding coefficients with the desired characteristic equation for the tracking error (8), the coefficients $q(\tau)$ and $p_i(\tau)$ are determined as

$$q(\tau) = c_n + \sum_{j=0}^{n-1} a_{11}^{j-n}(\tau)c_j, \quad p_i(\tau) = a_{12}(\tau)\sum_{j=0}^{i} a_{11}^{j-i-1}(\tau)c_j \tag{11}$$

where c_i's are determined based on the desired eigenvalue placement. Substitution of (11) into (7) represents the linear dynamic parameter-varying sliding manifold (7) as

$$\chi(t) = \eta(t) + \Omega(s)e(t) = 0 \tag{12}$$

where

$$\Omega(s) = \frac{a_{12}(\tau)\sum_{i=0}^{n-1}\sum_{j=0}^{i} a_{11}^{j-i-1}(\tau)c_j s^i}{s^{n+1} + c_n s^n + \sum_{j=0}^{n-1} a_{11}^{j-n}(\tau)c_j s^n}.$$

The conventional dynamic SMC can be constructed on the proposed sliding manifold (12) by

$$u(t) = -\Gamma \text{sign}(\chi(t)), \quad \Gamma > 0. \tag{13}$$

The conventional dynamic SMC (13), which operates on the time-varying dynamic sliding manifold (12), enables the system dynamics (1) to track the commanded AFR but with chattering effect, which is the main issue in SMC application. To tackle this problem, we will use the sliding manifold (12) in the following section to obtain a SOSMC that does not exhibit chattering behavior.

C. SOSMC of AFR

SOSMC is a modified version of the conventional SMC that drives the sliding variable and its first time derivative to zero in the presence of matched disturbance and uncertainties. Consider a second-order sliding manifold as

$$\ddot{\chi}(t) = -\alpha_m \text{sign}[\dot{\chi}(t)] - \alpha_M \text{sign}[\chi(t)] \tag{14}$$

where $\alpha_M > \alpha_m > 0$. As the time derivative of the sliding variable is not always measurable, indirect approaches like differentiators have been proposed to estimate the sliding variable time derivatives [22], [23]. However, to eliminate the need for such an additional dynamics, super-twisting SMC has been sought [24], [25]. Super-twisting sliding mode is a specific form of SOSMC law that relinquishes the need for the time derivative of the switching function and is described as

$$\begin{aligned} \dot{\chi}(t) &= -\alpha|\chi(t)|^{0.5}\text{sign}[\chi(t)] + \nu(t) \\ \dot{\nu}(t) &= -\gamma\,\text{sign}[\chi(t)] \end{aligned} \tag{15}$$

where α and $\gamma > 0$ are constants that should be determined.

To maintain the second-order sliding motion (15) on the dynamic sliding manifold (12), the following SOSMC is proposed in this paper:

$$\begin{aligned} u(t) &= -\alpha\Pi(s)|\chi(t)|^{0.5}\text{sign}[\chi(t)] + \Pi(s)\nu(t) \\ \dot{\nu}(t) &= -\gamma\,\text{sign}[\chi(t)] \end{aligned} \tag{16}$$

where $\Pi(s) = \beta^{-1}\Omega^{-1}(s)$ and $\beta = -\tau_s^{-1}$.

Theorem 1: The control law (16) provides the system represented by (5) with the second-order sliding motion on the parameter-varying dynamic switching manifold (12).

Proof: Consider the first time derivative of the dynamic switching manifold (12) as

$$\dot{\chi}(t) = \mu(t) + \Pi^{-1}(s)u(t) \tag{17}$$

where $\mu(t) = [a_{11} - a_{21}\Omega(s)]\eta(t) + [a_{12} - a_{22}\Omega(s)]\xi(t) + \Omega(s)\dot{y}^*(t) - \Omega(s)\phi_\xi(t) + \phi_\eta(t)$ is considered as a perturbation term, whose effect can be cancelled out by properly selecting the controller parameters α and γ. Substituting (16) into (17) yields the following dynamics:

$$\begin{aligned} \dot{\chi}(t) &= -\alpha|\chi(t)|^{0.5}\text{sign}[\chi(t)] + \nu(t) + \mu(t) \\ \dot{\nu}(t) &= -\gamma\,\text{sign}[\chi(t)]. \end{aligned} \tag{18}$$

We will consider the solution of (18) in the Fillipov sense [26]. Consider the state transformation $z(t) = [z_1(t), z_2(t)]^T = [|\chi(t)|^{0.5}\text{sign}[\chi(t)], \nu(t)]^T$. Equation (18) can be expressed in the new coordinate as

$$\dot{z}(t) = f[z_1(t)]z(t) + g[z_1(t)]\mu(t) \tag{19}$$

where

$$f[z_1(t)] = |z_1(t)|^{-1}\begin{bmatrix} -0.5\alpha & 0.5 \\ -\gamma & 0 \end{bmatrix}$$

$$g[z_1(t)] = |z_1(t)|^{-1}\begin{bmatrix} 0.5 \\ 0 \end{bmatrix}.$$

To prove the simultaneous convergence of z_1 and z_2 to zero, the following Lyapunov candidate function is considered:

$$V[z(t)] = z^T(t)Pz(t) \tag{20}$$

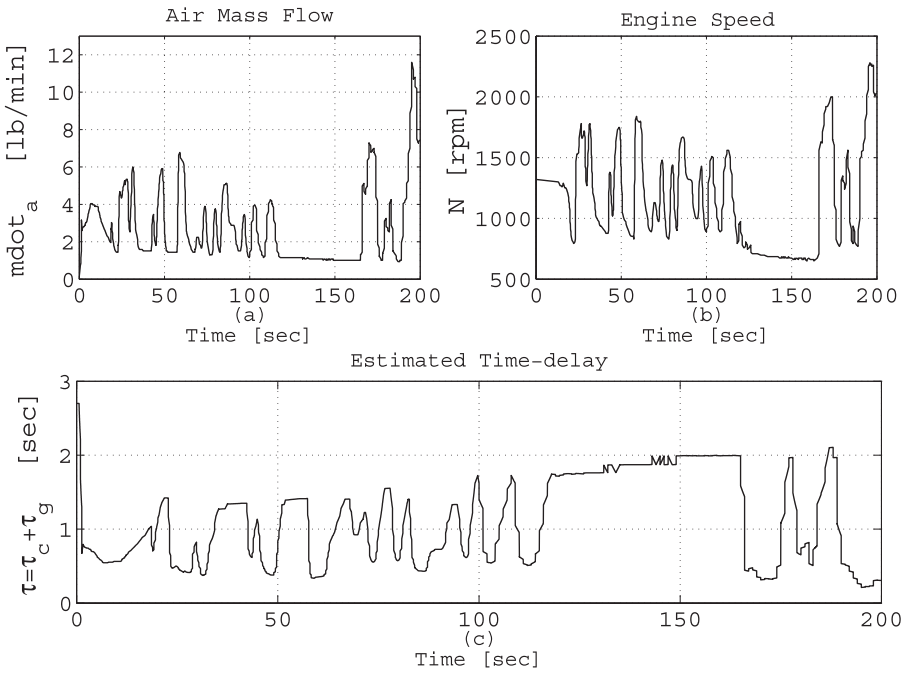

Fig. 4. (a) Air mass flow for the FTP. (b) Engine speed for FTP. (c) Estimated time-varying delay, $\tau = \tau_c + \tau_g$.

whose time derivative should meet the following criterion:

$$\dot{V}[z(t)] = \dot{z}^T(t)Pz(t) + z^T(t)P\dot{z}(t) \leq -|z_1(t)|^{-1}z^T(t)Qz(t) \tag{21}$$

where

$$P = \begin{bmatrix} p_{11} & p_{12} \\ p_{12} & p_{22} \end{bmatrix} \qquad Q = \begin{bmatrix} q_{11} & q_{12} \\ q_{12} & q_{22} \end{bmatrix}$$

are symmetric positive definite matrices. By substituting (19) into (21), following expression can be obtained

$$z^T(t)\bar{P}z(t) + \mu(t)\bar{p}^T z(t) \leq -z^T(t)Qz(t) \tag{22}$$

where

$$\bar{P} = \begin{bmatrix} -\alpha p_{11} - 2\gamma p_{12} & * \\ 0.5p_{11} - 0.5\alpha p_{12} - \gamma p_{22} & p_{12} \end{bmatrix}$$

and

$$\bar{p} = \begin{bmatrix} p_{11} \\ p_{12} \end{bmatrix}.$$

Moreover, by assuming $|\mu(t)| \leq \kappa|\chi(t)|^{0.5} = \kappa|z_1(t)|$ with $\kappa > 0$, (22) can be further expressed as

$$z^T(t)\bar{P}z(t) + \kappa|z_1(t)|\bar{p}^T z(t) \leq -z^T(t)Qz(t). \tag{23}$$

Using inequality $|z_1(t)|\bar{p}^T z(t) \leq p_{11}z_1^2 + |p_{12}||z_1(t)z_2(t)|$, (23) becomes

$$z^T(t)(\hat{P} + Q)z(t) \leq 0 \tag{24}$$

where for

$$z_1(t)z_2(t) > 0,\ \hat{P} = \begin{bmatrix} -\alpha p_{11} - 2\gamma p_{12} + \kappa p_{11} & * \\ 0.5p_{11} - 0.5\alpha p_{12} - \gamma p_{22} + 0.5\kappa|p_{12}| & p_{12} \end{bmatrix}$$

and for

$$z_1(t)z_2(t) < 0,\ \hat{P} = \begin{bmatrix} -\alpha p_{11} - 2\gamma p_{12} + \kappa p_{11} & * \\ 0.5p_{11} - 0.5\alpha p_{12} - \gamma p_{22} - 0.5\kappa|p_{12}| & p_{12} \end{bmatrix}.$$

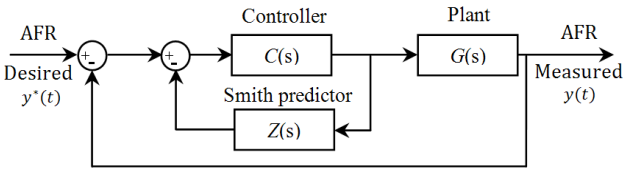

Fig. 5. Baseline controller configuration: a PI with Smith predictor.

However, choosing $\gamma \geq p_{22}^{-1}(q_{12} + 0.5p_{11} - 0.5\alpha p_{12} + 0.5\kappa|p_{12}|)$ and $\alpha \geq p_{11}^{-1}(q_{11} - 2\gamma p_{12} + \kappa p_{11})$ ensures negative definiteness of matrix $\hat{P} + Q$ for the two possible cases of $\hat{P}$. This maintains the convergence of $z_1(t)$ and $z_2(t)$ to zero, which leads to $\chi(t), \dot{\chi}(t) \to 0$ and proves the theorem. □

The presented SOSMC (16), which operates on the time-varying dynamic sliding manifold (12), enables the system dynamics (1) to track the commanded AFR with no chattering effect. This will be demonstrated in the following section by comparing it with a conventional dynamic sliding mode controller (13).

IV. Results and Discussion

The results of simulation of the proposed SOSMC on the linear dynamic parameter-varying sliding manifold (12) are presented in this section. Various operating conditions including perturbations and sensor noise are considered. The closed-loop simulations were conducted using experimental federal test procedure (FTP) air mass flow and RPM data collected on a Ford truck F-150 4.6L V8 engine at the University of Houston's Engine Control Research Laboratory [3].

The internal dynamics (5a) can be rearranged as

$$\dot{\eta}(t) = 2\tau^{-1}\eta(t) + \tau_s e(t) + \bar{\phi}_\eta(t) \tag{25}$$

where $e(t) = y^*(t) - y(t)$ and $\bar{\phi}_\eta(t) = -\tau_s y^*(t) + \phi_\eta(t)$. By treating the AFR control as a regulation problem and further assuming that $\dot{\bar{\phi}}_\eta(t) = 0$, i.e., $k = 1$, the linear dynamic

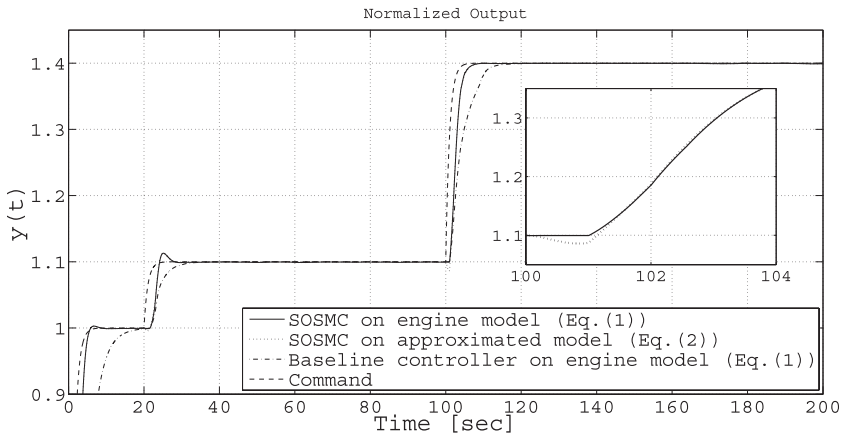

Fig. 6. Closed-loop system performance for the actual system (solid line) and the approximated nonminimum phase system (dotted line) using the designed SOSMC and the actual system with the baseline controller (dashed-dotted line).

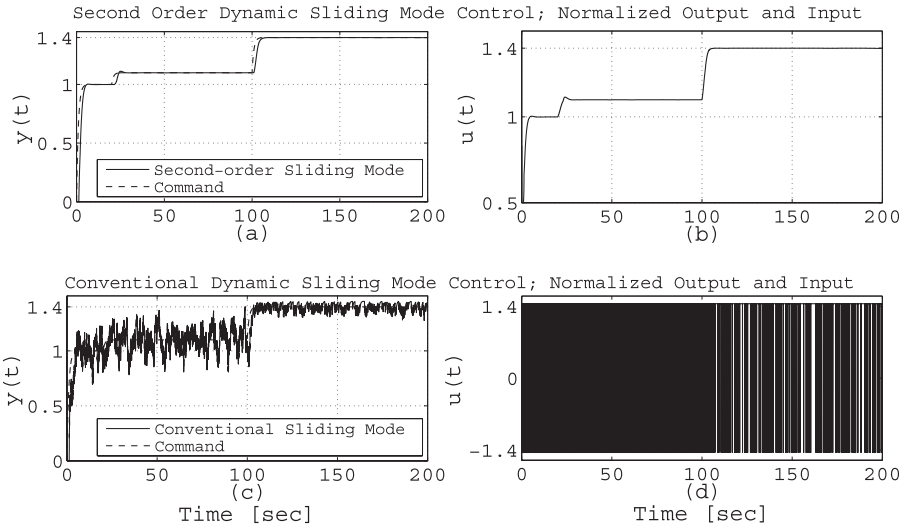

Fig. 7. (a) Closed-loop system performance corresponding to the SOSMC. (b) SOSMC input. (c) Closed-loop system performance corresponding to the conventional dynamic SMC. (d) Conventional dynamic SMC input.

parameter-varying sliding manifold (12) can be represented in the following form for a desired second-order error dynamics, i.e., $n = 1$

$$\chi(t) = \eta(t) + \frac{p_0(\tau)}{s^2 + q(\tau)s} e(t) = 0. \tag{26}$$

Substituting (26) into (25) and choosing the desired characteristic equation $\ddot{e} + 1.4\dot{e} + e = 0$ yields $p_0(\tau) = -0.5\tau_s\tau$ and $q(\tau) = 1.4 + 0.5\tau$. Consequently, the dynamic operator of (7) is obtained as $\Omega(s) = -1/2\tau_s\tau/[s^2 + (1.4 + 0.5\tau)s]$. Hence, the associated sliding manifold (12) is rewritten as

$$\chi(t) = \eta(t) - \frac{1}{2}\frac{\tau_s\tau}{s^2 + (1.4 + 0.5\tau)s} e(t) = 0. \tag{27}$$

The root locus plot in Fig. 3 shows how the unstable internal dynamics (5a) performs on the switching surface (27) for a sequence of delay variations 0.3s $\leq \tau \leq$ 2.7 s with an increment of 0.1 s. It can be observed that as the delay increases the root loci are scaled smaller with limited closed-loop performance. For instance, the attainable gain for the lowest delay is $K|_{\tau=0.3} = 10.2$, which is five times higher than the gain for the largest delay $K|_{\tau=2.7} = 2.03$. The associated frequencies for the lowest and highest delays are $\omega|_{\tau=0.3} = 3.2$ rad/s and $\omega|_{\tau=2.7} = 1.4$ rad/s. This implies a lower bandwidth for the larger delays and vice versa. Hence, designing a controller whose parameters vary as time delay changes can extend the bandwidth when the system experiences short delays.

The collected data are engine air mass flow and engine RPM, as shown in Fig. 4(a) and (b), respectively. The engine air mass flow is used to obtain the gas transport delay by $\tau_g = \vartheta/\dot{m}_a$ with $\vartheta = 1.81$ and the engine RPM is used to obtain the cycle delay according to $\tau_c = 120/N$. The overall time-varying delay, thus, can be shown in Fig. 4(c) for 0.3s $\leq \tau \leq$ 2.7s. It is assumed that the engine is commanded to operate at normalized lean AFR, typically 1.1 or 1.4. The simulations are performed in MATLAB/Simulink using Runge–Kutta ODE4 for numerical integration.

The closed-loop system response is evaluated next against a baseline controller shown in Fig. 5. The baseline controller is a PI controller, $C(s) = K_p(1 + 1/Ts)$, combined with a parameter-varying Smith predictor, $Z(s) = 1/(\tau_s s + 1)(1 - e^{-\tau s})$, to compensate for the large delays. The parameter T is chosen equal to the lag of the system τ_s. The integrator maintains robustness against step disturbances and leads to a first-order set point response with time constant $1/K_p$ [27].

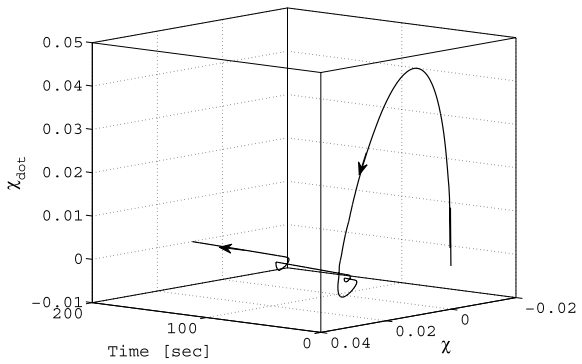

Fig. 8. Twisting motion of the second-order sliding mode approach.

However, very large values of K_p make the closed-loop system unstable due to the delay and the amplification of the measurement noise.

Fig. 6 shows the closed-loop system response for the actual system (solid line) and the approximated nonminimum phase system (dotted line) using the designed SOSMC and the actual system with the baseline controller (dash-dotted line). The controller parameters have been considered as $\alpha = 3$ and $\gamma = 0.001$, which also satisfy the bounds given in Section III-C. The undershoot for the nonminimum phase system in the magnified graph in Fig. 6 is less than 5%. The controller can perform well on the actual system (1) and overlaps well with the nonminimum phase system response. The settling time for the proposed controller is 8s, which is considerably lower than the settling time of 17s for the baseline controller. It is shown than the proposed controller can perform well with fast convergence response.

The system closed-loop response has been shown against conventional dynamic SMC in Fig. 7. Fig. 7(a) shows the actual delay with the corresponding SOSMC shown in Fig. 7(b). The conventional dynamic SMC performance with chattering effect, which is an intrinsic characteristic of classical SMC, has been shown in Fig. 7(c) based on the sliding manifold (27). The associated switching control input has been shown in Fig. 7(d). Unlike the conventional dynamic SMC, which suffers from the chattering phenomena, the SOSMC leads to a chatter-free response with no further need for chattering-suppression techniques developed so far for SMC theory.

Fig. 8 shows the twisting motion in the phase plane. Starting from the initial setting, the system motion is to diminish the switching function χ and its derivative $\dot{\chi}$ in (18).

The closed-loop system response against external disturbance including fuel injector and canister purge disturbance has been shown in Fig. 10 with the disturbance profile as in Fig. 9. The proposed controller shows very fast response compared with the baseline controller against the disturbance profile. To further evaluate the robustness of the proposed controller, various delay estimation errors are considered as: 1) nominal delay (solid line); 2) 20% time delay overestimation (dotted line); and 3) 20% time delay underestimation (dash-dotted line). It is shown in Fig. 11 that the closed-loop system is robust against open-loop fuel injector and canister purge disturbance and delay variations. However, for overestimated delays, the controller exhibits large-amplitude

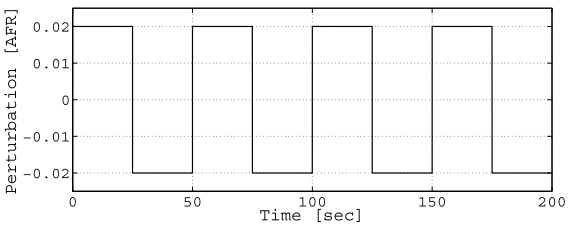

Fig. 9. Typical disturbance profile for the fuel injector and canister purge disturbance.

oscillations while attenuating the disturbance. This is due to the induced lower bandwidth by the overestimated delay, which reduces the system damping and thus allows for transient oscillations.

Fig. 12(a) shows the closed-loop system performance in the presence of the time-varying delay, open-loop disturbance, and the UEGO sensor measurement noise. The measurement noise is assumed to be a white noise signal with a power intensity of 10^{-4}, which produces a noise with amplitude of 5% in the sensor output. The magnified graph within Fig. 12(a) shows that the controller has attenuated the noise signal more effectively and faster than the baseline controller. From Fig. 12(b), the corresponding control input for the SOSMC operates with lower noise amplitude compared with the baseline controller.

Furthermore, the effect of wall wetting and fuel vaporization is considered using a model for the fuel-path dynamics as

$$\ddot{m}_{fo} + \frac{1}{\tau_f}\dot{m}_{fo} = (1 - X)\ddot{m}_{fi} + \frac{1}{\tau_f}\dot{m}_{fi} \tag{28}$$

where X is the fraction of injected fuel that forms a wet film on the walls, τ_f is the time constant for the evaporated fuel from the wet wall, and $\dot{m}_{fi}$ and $\dot{m}_{fo}$ are the injected fuel flow rate into the fueling chamber and output flow rate delivered into the ignition chamber, respectively [18]. The parameters of the fueling dynamics are considered to be $\tau_f = 0.1$ s and $X = 0.5$ (assuming that half of the injected fuel forms a wet film on the walls) [18]. Fig. 13(a) shows that the effect of the fuel-path dynamics (the difference between the reference tracking with and without fuel-path dynamics) on the closed-loop response is negligible. Fig. 13(b) shows that the effect of the fuel-path dynamics on the corresponding control input is also negligible.

During lean operation, the exhaust catalyst is saturated with oxygen and its dynamics is dominated by the time-varying delay. Lean-burn engines switch from lean to rich and vice versa for purging purposes. After switching from lean to rich, the postcatalyst lambda remains at $\lambda = 1$ for a few seconds to deplete the stored oxygen and then moves to $\lambda < 1$ (rich). Similar effect takes place upon switching from rich to lean. This nonlinear behavior has a significant influence on the control system behavior. The examination of the switching dynamics of the catalytic converter and its effect on the design of the control system are discussed in [28] and [29]. Fig. 14(a) shows the robustness of the proposed controller when the operation is switching from lean to rich and vice versa. We have included two switchings corresponding to the lower and upper delays at $t = 70$ s and $t = 140$ s [see Fig. 4(c)]. The first lean-to-rich switching

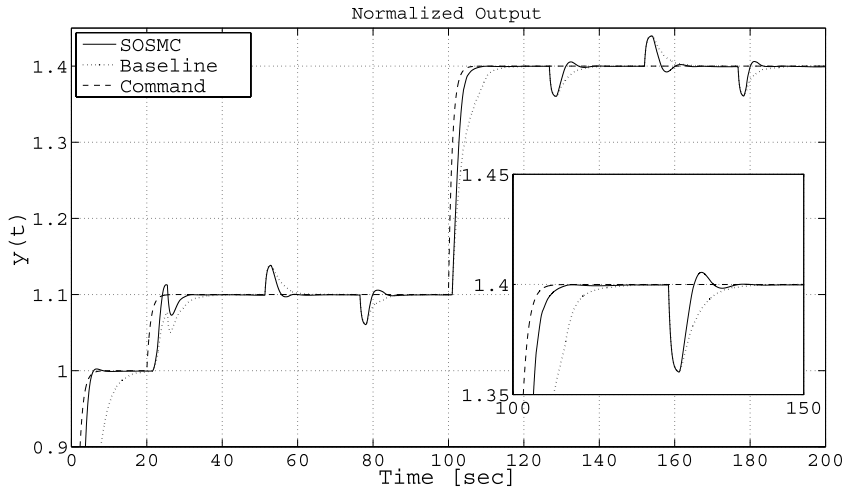

Fig. 10. Closed-loop performance of the second-order sliding mode scheme compared with the baseline controller.

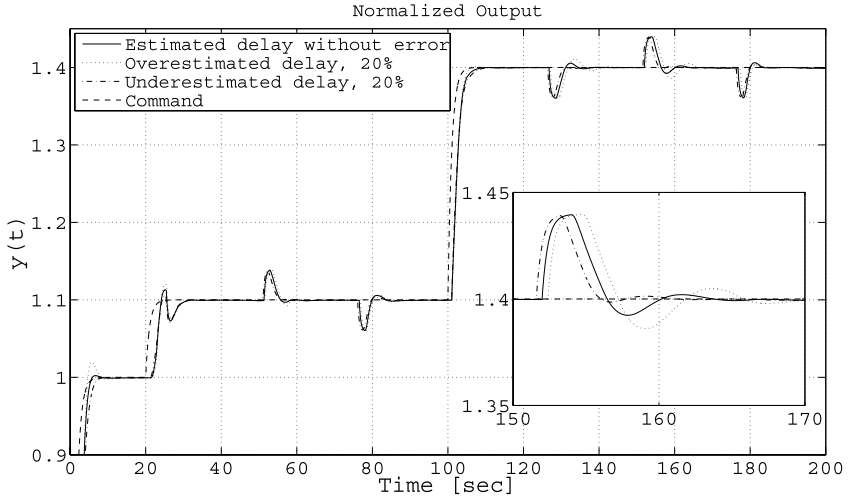

Fig. 11. Closed-loop performance of the SOSMC in the presence of the fuel injector and canister purge disturbance and various delay estimation errors.

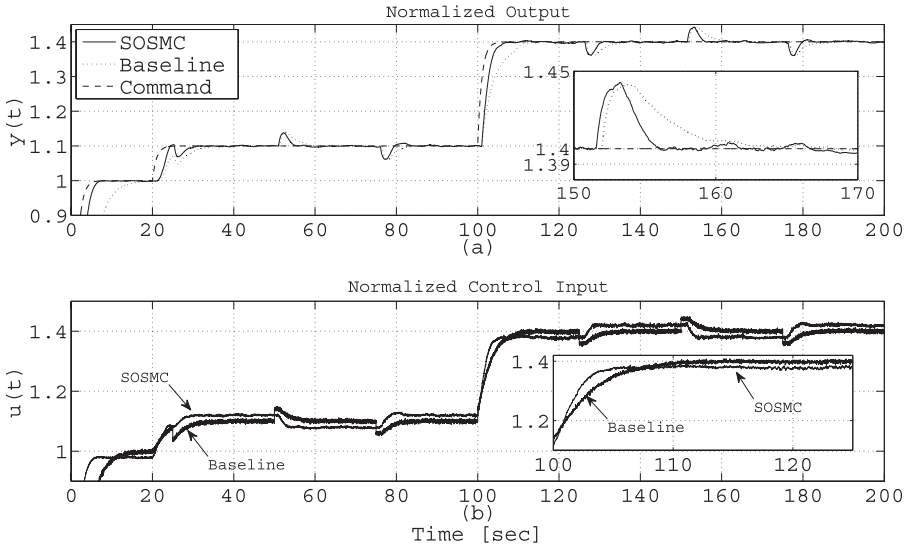

Fig. 12. (a) Output tracking with time-varying delay in the presence of the measurement noise and the fuel injector and canister purge disturbance for the second-order sliding mode and baseline controllers. (b) Corresponding control inputs.

occurring at $t = 70$ s shows no overshoot due to the lower delay, whereas for the second switching at $t = 140$ s, the response exhibits 5% overshoot because of larger time delay. The corresponding control input has been shown in Fig. 14(b), which demonstrates the controller robustness against lean-rich switching.

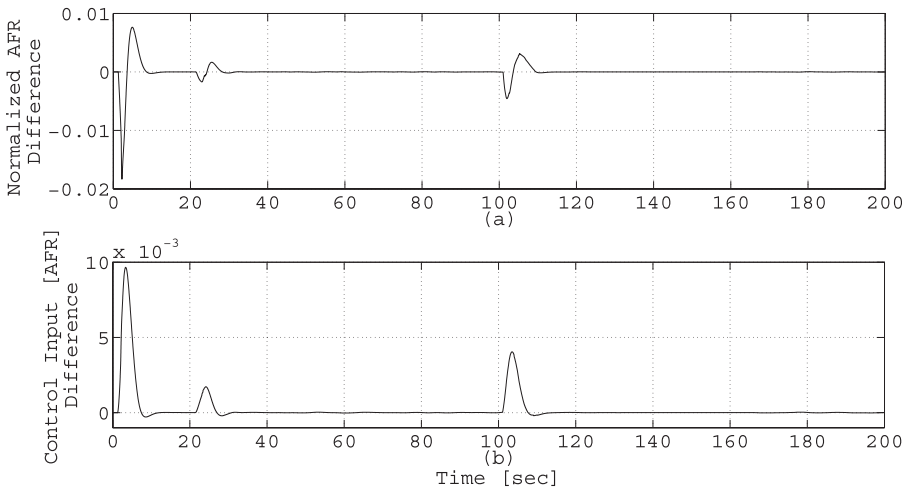

Fig. 13. (a) Difference between the reference tracking with and without fuel-path dynamics for the time-varying delay. (b) Difference between the corresponding control input with and without fuel-path dynamics.

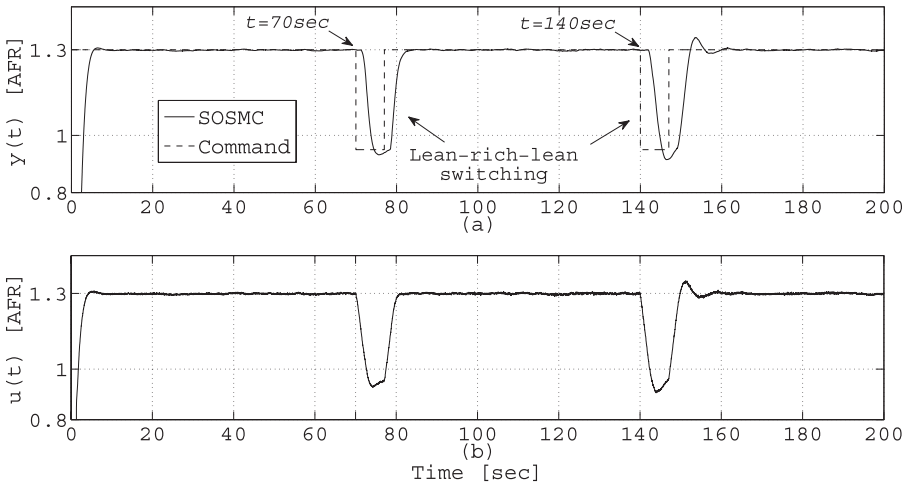

Fig. 14. (a) Reference tracking with time-varying delay in the presence of measurement noise and lean-to-rich/rich-to-lean switching of the engine for depletion of the stored oxygen in the catalyst. (b) Corresponding control input.

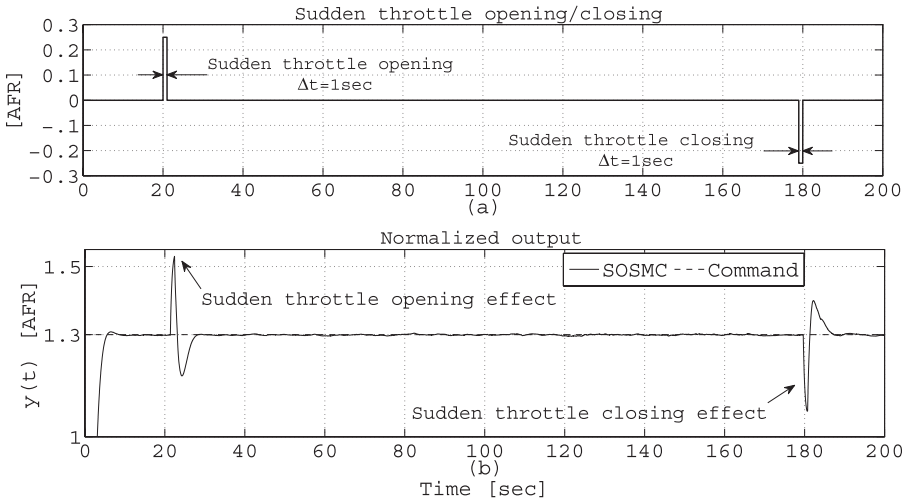

Fig. 15. (a) Profiles of the sudden opening and closing of the throttle. (b) Effect of sudden throttle opening and closing on output tracking in the presence of measurement noise.

Moreover, Fig. 15 shows the effect of sudden throttle opening and closing. Sudden throttle opening is usually accompanied by a lean spike in the AFR, whereas sudden throttle valve closing is followed by a rich AFR. To include the effect of sudden throttle changes, we considered a pulse-shaped disturbance signal with 25% of the nominal AFR amplitude and duration of 1 s ($\Delta t = 1$ s) at $t = 20$ s and $t = 180$ s, as shown in Fig. 15(a). The sudden throttle opening

and closing in Fig. 15(b) show 15% increase and decrease in the lean operation of the engine, respectively.

V. Conclusion

A SOSMC strategy was presented to control AFR in lean-burn spark-ignition engines with large time-varying delay. The engine dynamics with time-varying delay were represented in the form of a parameter-dependent nonminimum phase system using the Padé approximation. The system dynamics were further rendered into the normal form to investigate the unstable internal dynamics. A linear dynamic parameter-varying sliding manifold with straightforward approach to derive its parameters was used to compensate for the unstable internal dynamics of the nonminimum phase system. The order of the switching manifold could be determined based on the desired error dynamics to regulate the closed-loop system response. The SOSMC was then presented for the dynamic parameter-varying sliding manifold, which resulted in a chattering-free closed-loop system response compared with the presented conventional dynamic sliding mode controller with high chattering effect. The results demonstrated a good match for the dynamic model of the lean-burn engine with that of the approximated nonminimum phase system. Furthermore, the proposed controller achieved a superior performance compared with the baseline controller with an embedded Smith predictor. The results showed that the control system was able to attenuate the effect of fuel injector and canister purge uncertainties. Moreover, the control system exhibited robustness against various delay overestimation and underestimation errors. It was observed that the closed-loop system demonstrated an excellent performance against the UEGO sensor noise by attenuating noise effect on the AFR output tracking. Finally, the closed-loop response of the system was evaluated against fuel-path dynamics, lean-to-rich and rich-to-lean switchings and sudden throttle changes. It should be noted that the proposed controller can be applied to other systems with similar structure. Unlike GS approaches, the proposed design method does not require additional computational efforts for the parameter-varying sliding manifold as only a few multiplications and additions are performed to obtain the varying parameters. It is expected that the proposed SOSMC of AFR in IC engine lean operation would lead to fuel economy and emission reduction improvements. Quantification of the improvements on an experimental test bed will be pursued in a future study.

References

[1] J. Powel, N. Fekete, and C.-F. Chang, "Observer-based air-fuel ratio control," *IEEE Control Syst. Mag.*, vol. 18, no. 5, pp. 72–81, Oct. 1998.

[2] L. Mianzo, H. Peng, and I. Haskara, "Transient air-fuel ratio H_∞ preview control of a drive-by-wire internal combustion engine," in *Proc. Amer. Control Conf.*, 2001, pp. 2867–2871.

[3] F. Zhang, K. Grigoriadis, M. Franchek, and I. Makki, "Linear parameter-varying lean burn air-fuel ratio control for a spark ignition engine," *ASME J. Dyn. Syst., Meas., Control*, vol. 129, pp. 404–414, Jul. 2007.

[4] B. Ebrahimi, R. Tafreshi, M. Masudi, M. Franchek, J. Mohammadpour, and K. Grigoriadis, "A parameter-varying filtered PID strategy for air-fuel ratio control of spark ignition engines," *Control Eng. Pract.*, vol. 20, no. 8, pp. 805–815, 2012.

[5] A. Kwiatkowski, H. Werner, J. P. Blath, A. Ali, and M. Schultalbers, "Linear parameter varying PID controller design for charge control of a spark-ignited engine," *Control Eng. Pract.*, vol. 17, no. 11, pp. 1307–1317, 2009.

[6] K. R. Muske, J. C. P. Jones, and E. M. Franceschi, "Adaptive analytical model-based control for SI engine air-fuel ratio," *IEEE Trans. Control Syst. Technol.*, vol. 16, no. 4, pp. 763–768, Jul. 2008.

[7] A. White, J. Choi, R. Nagamune, and G. Zhu, "Gain-scheduling control of port-fuel-injection processes," *Control Eng. Pract.*, vol. 19, no. 4, pp. 380–394, 2011.

[8] D. Cho and J. K. Hedrick, "A nonlinear controller design method for fuel-injected automotive engines," *J. Eng. Gas Turbines Power*, vol. 110, no. 3, pp. 313–320, 1988.

[9] S. B. Choi and J. K. Hedrick, "An observer-based controller design method for improving air/fuel characteristics of spark ignition engines," *IEEE Trans. Control Syst. Technol.*, vol. 6, no. 3, pp. 325–334, May 1998.

[10] J. S. Souder and J. K. Hedrick, "Adaptive sliding mode control of air-fuel ratio in internal combustion engines," *Int. J. Robust Nonlinear Control*, vol. 14, no. 6, pp. 525–541, 2004.

[11] S. Pace and G. G. Zho, "Air-to-fuel and dual-fuel ratio control of an internal combustion engine," *SAE Int. J. Eng.*, vol. 2, no. 2, pp. 245–253, 2009.

[12] S. Wang and D. L. Yu, "A new development of internal combustion engine air-fuel ratio control with second-order sliding mode," *ASME J. Dyn. Syst., Meas., Control*, vol. 129, no. 6, pp. 757–766, 2007.

[13] J. Lauber, T. M. Guerra, and M. Dambrine, "Air-fuel ratio control in a Gasoline engine," *Int. J. Syst. Sci.*, vol. 42, no. 2, pp. 277–286, 2011.

[14] Y. Yildiz, A. M. Annaswamy, D. Yanakiev, and I. Kolmanovski, "Spark ignition engine air-to-fuel ratio control: An adaptive control approach," *Control Eng. Pract.*, vol. 18, pp. 1369–1378, Jul. 2010.

[15] C. Beltrami Y. Chamaillard, G. Miller, P. Higelin, and G. Bloch, "AFR control in SI engine with neural prediction of cylinder air mass," in *Proc. Amer. Control Conf.*, 2003, pp. 1404–1409.

[16] Q. R. Butt and A. I. Bhatti, "Estimation of Gasoline engine parameters using higher order sliding mode," *IEEE Trans. Ind. Electron.*, vol. 55, no. 11, pp. 3891–3898, Nov. 2008.

[17] V. K. Jones, B. A. Ault, G. F. Franklin, and J. V. Powell, "Identification and air-fuel ratio control of a spark ignition engine," *IEEE Trans. Control Syst. Technol.*, vol. 3, no. 1, pp. 14–21, Mar. 1995.

[18] Y.-Y. Wu, B.-C. Chen, F.-C. Hsieh, and C.-T. Ke, "A study of the characteristics of fuel-film dynamics for four-stroke small-scale spark-ignition engines," Dept. Veh. Eng., Nat. Taipei Univ. Technol., Chinese, Taipei, Taiwan, Tech. Rep. SAE Paper 2009-01-0591, 2009.

[19] M. A. Franchek, J. Mohrfeld, and A. Osburn, "Transient fueling controller identification for spark ignition engines," *ASME J. Dynamic Syst., Meas., Control*, vol. 128, no. 3, pp. 499–509, 2006.

[20] A. Isidori, *Nonlinear Control Systems*, 3rd ed., New York, NY, USA: Springer-Verlag, 1995.

[21] I. A. Shkolnikov and Y. B. Shtessel, "Aircraft nonminimum phase control in dynamic sliding manifolds," *J. Guid., Control, Dyn.*, vol. 24, no. 3, pp. 566–572, 2001.

[22] A. Levant, "Higher-order sliding modes, differentiation and output feedback control," *Int. J. Control*, vol. 76, nos. 9–10, pp. 924–941, 2003.

[23] A. Levant, "Principle of 2-sliding mode control," *Automatica*, vol. 43, pp. 576–586, May 2007.

[24] J. Davila, L. Fridmann, and A. Levant, "Second-order sliding-mode observer for mechanical systems," *IEEE Trans. Autom. Control*, vol. 50, no. 11, pp. 1785–1789, Nov. 2005.

[25] Y. B. Shtessel, J. A. Moreno, F. Plestan, L. M. Fridman, and A. S. Poznyak, "Super-twisting adaptive sliding mode control: A Lyapunov design," in *Proc. 49th IEEE Conf. Decision Control*, Dec. 2010, pp. 5109–5113.

[26] A. F. Fillipov, *Differential Equations with Discontinuous Right-Hand Side*. Boston, MA, USA: Kluwer, 1988.

[27] Q. C. Zhong, *Robust Control of Time-delay Systems*, New York, NY, USA: Springer-Verlag, 2006.

[28] J. C. P. Jones, J. B. Roberts, P. Bernard, and R. A. Jackson, "A simplified model for the dynamics of a three-way catalytic converter," Dept. Eng. Appl. Sci., Sussex Univ., Sussex, U.K., Tech. Rep. SAE Paper 2000-01-0652, 2000.

[29] E. P. Brandt, W. Yanying, and J. W. Grizzle, "Dynamic modeling of a three-way catalyst for SI engine exhaust emission control," *IEEE Trans. Control Syst. Technol.*, vol. 8, no. 5, pp. 767–776, Jan. 2000.

Behrouz Ebrahimi (M'11) received the B.S.M.E. degree from the University of Tabriz, Tabriz, Iran, in 2000, the M.S.M.E. and Ph.D. degrees from the Amirkabir University of Technology (Tehran Polytechnic), Tehran, Iran, in 2002 and 2009, respectively.

He was a Post-Doctoral Research Associate with Texas A&M University at Qatar, Doha, Qatar, from 2011 to 2013, where he developed robust parameter-varying control strategies to reduce tail-pipe emission of spark ignition engines with time-varying delay in the control loop. His current research interests include robust and nonlinear controller/observer design, distributed and decentralized modeling and control, system identification, model based fault detection, and diagnostics.

Dr. Ebrahimi received the 2013 Research Excellence Award.

Reza Tafreshi (M'05) received the B.Sc. and M.Sc. degrees from the K.N. Toosi University of Technology, Tehran, Iran, in 1991 and 1995, respectively, and the Ph.D. degree in mechanical engineering from the University of British Columbia (UBC), Vancouver, BC, Canada, in 2005.

He was with PoloDej Company, Tehran, from 1995 to 1999. From 1999 to 2000, he was a Research Engineer with the Department of Electrical Communication Engineering, UBC. He was a Visiting Assistant Professor with Texas A&M University, College Station, TX, USA, in 2006. In 2007, he joined Texas A&M University at Qatar, Doha, Qatar, where he is currently an Assistant Professor. His current research interests include controls, machine fault diagnosis, condition monitoring, and biomedical engineering.

Javad Mohammadpour (M'05) received the B.S. and M.S. degrees in electrical engineering and the Ph.D. degree in mechanical engineering.

He joined the University of Georgia, Atlanta, GA, USA, as an Assistant Professor of electrical engineering in 2012. He was with the Naval Architecture and Marine Engineering Department, University of Michigan, Ann Arbor, MI, USA, as a Research Scientist, from October 2011 to July 2012. He was a Research Assistant Professor of mechanical engineering with the University of Houston, Houston, TX, USA, from October 2008 to September 2011. He has published over 80 articles in international journals and conference proceedings, served as a PI or co-PI in several funded projects, served in the editorial boards of ASME and IEEE conferences on control systems and edited two books on *Control of Large-Scale Systems* and *LPV Systems Modeling, Control and Applications*.

Matthew Franchek (M'94) received the B.S.M.E. degree in 1987 from the University of Texas at Arlington, Arlington, TX, USA, in 1987, and the M.S.M.E. and Ph.D. degrees from Texas A&M University, College Station, TX, USA, in 1988 and 1991, respectively.

He is a Professor with the Department of Mechanical Engineering, University of Houston, Houston, TX, USA. His current research interests include developing of the science and technology of designing nonlinear and multivariable controllers for internal combustion engine engines, exhaust after-treatment components, subsea drilling and production systems, noise/vibration control of structures, and health prognostics of cardiovascular and respiratory systems.

Karolos Grigoriadis (SM'13) received the Ph.D. degree in aeronautics and astronautics from Purdue University, West Lafayette, IN, USA, in 1994.

He is currently a Professor of mechanical engineering and the Director of the Aerospace Engineering Program, University of Houston, Houston, TX, USA. He has been an Honorary Visiting Professor with Loughborough University, Loughborough, U.K., since 2008. His expertise is on the modeling, analysis, design optimization and control of mechanical, aerospace, biomedical and energy systems. He has authored or co-authored over 150 journal and proceeding articles, three book chapters, and three books. He has organized several invited sessions, workshops, and short-courses at national and international conferences, and he has been in the editorial board of international journals and international conference committees in the systems and controls area.

Dr. Grigoriadis is the recipient of several national and university awards, including the National Science Foundation CAREER Award, the Society of Automotive Engineers Ralph Teetor Award, the Bill Cook Scholar Award, the Herbert Allen Award for Outstanding Contributions by a Young Engineer and Multiple Research Excellence, and the Teaching Excellence Awards.

Houshang Masudi is a Professor of the Mechanical Engineering Program, Texas A&M University at Qatar, Doha, Qatar. He has a great deal of experience as a Researcher, Educator and Service Provider at national and international levels. He has developed and organized a number of technical programs and workshops for the Energy Sources Technology Conference and Exhibition, ASME ASIA Congress and Exhibition in 1997, ASME European Joint Conference on System Design and Analysis, and Integrated Design and Process Technology Conference.

He is the recipient of numerous awards for teaching excellence and professional services. He is a member of Beta Alpha Phi (International Honor Society), Tau Beta Pi (Engineering Honor Society), Pi Tau Sigma (Mechanical Engineering Honor Society), and Life Member of ASME and ASEE.